JOURNAL OF GEOPHYSICAL RESEARCH, VOL. 102, NO. D17, PAGES 21,431–21,442, SEPTEMBER 20, 1997

NO_x emission indices of subsonic long-range jet aircraft at cruise altitude: In situ measurements and predictions

P. Schulte, H. Schlager, H. Ziereis, and U. Schumann

Deutsche Forschungsanstalt für Luft- und Raumfahrt, Institut für Physik der Atmosphäre, Oberpfaffenhofen Germany

S. L. Baughcum

Boeing Company, Seattle, Washington

F. Deidewig

Deutsche Forschungsanstalt für Luft- und Raumfahrt, Institut für Antriebstechnik, Cologne, Germany

Abstract. In the course of the Commissions of the European Communities project "Pollution From Aircraft Emissions in the North Atlantic Flight Corridor (POLINAT)", in situ measurements of NO, NO_x, and CO_2 volume mixing ratios in the near-field exhaust plumes of seven subsonic long-range jet aircraft have been carried out by using the research aircraft *Falcon* of the Deutsche Forschungsanstalt für Luft- und Raumfahrt (DLR). For three additional aircraft, only NO and CO_2 were measured. Plume ages of 50 s to 150 s have been covered, with maximum observed exhaust gas enhancements of 319 parts per billion by volume and 51 parts per million by volume for $\Delta[NO_x]$ and $\Delta[CO_2]$, respectively, in relation to ambient values. Aircraft cruising altitudes and Mach numbers ranged from 9.1 to 11.3 km and from 0.77 to 0.85, respectively. These measurements are used to derive NO_x emission indices for seven of the individual aircraft/engine combinations. The NO_x emission indices derived range from 12.3 g/kg to 30.4 g/kg. They are compared with predicted emission index values, calculated for the same aircraft engine and the actual conditions by using two newly developed fuel flow correlation methods. The calculated emission indices were mostly within or close to the error limits of the measured values. On average, the predictions from both methods were 12% lower than the measured values, with an observed maximum deviation of 25%. The ratio $\gamma = [NO_2]/[NO_x]$ found during the present measurements ranged from 0.06 to 0.11 for five daytime cases and was around 0.22 for two nighttime cases. By use of a simple box model of the plume chemistry and dilution these data were used to estimate the initial value γ_0 present at the engine exit plane. We found γ_0 values between 0 and 0.15. These were applied to estimate the corresponding NO_2 for the three cases in which only NO was measured.

Introduction

In the upper troposphere and lower stratosphere, air traffic represents an important anthropogenic source of trace gases [*Schumann*, 1994]. Especially at northern midlatitudes, where air traffic is most intense, the amount of NO_x resulting from aircraft is predicted to be comparable with the important natural sources (lightning, downward transport from the stratosphere, and fast vertical transport from the surface via strong convection during thunderstorm) [*Ehhalt et al.*, 1992; *Köhler et al.*, 1996]. This increase in upper tropospheric/lower stratospheric NO_x could lead to ozone production, which in turn would add to the atmospheric greenhouse effect [*Johnson et al.*, 1992; *Beck et al.*, 1992; *Brasseur et al.*, 1996].

For global models to be able to assess the possible climate effects of NO_x emitted by the worldwide fleet of aircraft, an emission inventory of the amount of NO_x produced by air traffic is needed. NO_x emission inventories are constructed by combining an aircraft movement database with typical flight profiles (for example, engine power setting or fuel flow as a function of time) and information on the specific emission of the individual aircraft/engine combinations [*McInnes and Walker*, 1992; *Wuebbles et al.*, 1993; *Baughcum et al.*, 1996; *Gardner et al.*, 1997].

The specific emission of NO_x produced by a certain engine type is usually given in terms of an NO_x emission index, $EI(NO_x)$, which specifies the amount of NO and NO_2 as equivalent grams of NO_2 produced by burning 1 kg of fuel. $EI(NO_x)$ values of most engines presently in use have

Paper number 97JD01526.
0148-0227/97/97JD-01526$09.00

been measured during the certification procedure on ground test facilities for a fixed set of engine power settings and are tabulated by the *International Civil Aviation Organisation (ICAO)* [1995]. However, these measurements were carried out under static sea level pressure and temperature conditions, whereas in cruise flight the engines are operated at much lower pressures and temperatures, leading to different emission indices. Therefore one has to rely on prediction methods that extrapolate from emission indices measured on ground to the actual altitude values. Several different prediction methods are presently in use, leading to considerably different results (for an overview see *Lister et al.* [1995]). It was suspected that, among other possible reasons, this factor might be a significant contributor to the differences in existing emission inventories. In an intercomparison in terms of a global NO_x emission index (annual global aircraft produced amount of NO_x per annual fuel consumed globally by aircraft), one learns, for example, that *Wuebbles et al.* [1993] found 10.9 g/kg for the inventory and *Gardner et al.* [1997] found 16.8 g/kg.

EI(NO_x) prediction methods can be devided into two categories: (1) relative correlations, and (2) fuel flow methods. The former methods depend on knowledge of engine specific parameters as, for example, the combustor inlet temperature and pressure, which are proprietary to the engine manufacturers and not publically available. If these parameters are known for ground conditions, they can be calculated very accurately for given altitude conditions by thermodynamical engine modeling. However, such calculations would be necessary for a great variety of aircraft/engine combinations, ambient conditions at altitude, and flight profiles (actual aircraft weight, Mach number and other variables, as a function of time).

In contrast, fuel flow methods only need information on ambient temperature, pressure, humidity, actual fuel flow, and Mach number of the aircraft to infer cruise emission indices from the ICAO values. They can be considered as empirical interpolations, representing a best fit to the results of the relative correlation methods and have been developed for use in recent emission inventories [*Baughcum et al.*, 1996]; Deutsche Forschungsanstalt für Luft- und Raumfahrt (DLR), unpublished emission inventory, 1997; European Civil Aviation Conference/Abatement of Nuisance Caused by Air Transport & European Community (ECAC/ANCAT & EC) Working Group, unpublished emission inventory, 1997]. These represent improved versions of the inventories by *Wuebbles et al.* [1993] and *Gardner et al.* [1997], but there still exists a difference of about 25% in terms of their resulting effective global NO_x emission indices (A. Schmitt, personal communication, 1996). Therefore a validation of the two prediction methods applied in the recent studies is desirable.

In principle, cruise condition emission indices can be measured on high-altitude simulation test facilities, but such measurements are expensive, and thus only a few data sets are available for selected engines [*Lister et al.*, 1995]. Alternatively, the relevant emission indices can be measured in situ by direct sampling of engine emissions in the source aircraft exhaust plume. First measurements of this kind have been reported only recently: *Arnold et al.* [1992] reported the first measurements of [NO], [NO_2], [HNO_2], and [HNO_3] in the young exhaust plume of a DC-9 at cruise (plume age 9 s), using chemical ionization mass spectrometry. The data, corrected for uncertainties in the ion reaction rates, show an [NO_2]/[NO_x] ratio of 0.2 to 0.3, consistent with the measured [HNO_3]/[HNO_2] ratio of about 1. *Fahey et al.* [1995a] determined the NO_x emission index of the ER-2 engine (P&W J75) in the lower stratosphere and found excellent agreement with values based on a prediction method from the engine manufacturer, Pratt & Whitney. In another study, *Fahey et al.* [1995b] measured EI(NO_x) of the Concorde supersonic aircraft engines in the lower stratosphere. *Schulte and Schlager* [1996] performed NO and CO_2 measurements in the exhaust plumes of commercial short- to medium-range aircraft at cruise altitude and derived lower limits of EI(NO_x) that are in good agreement with values obtained by use of two fuel flow based prediction methods.

Here for the first time, in situ NO_x emission index measurements of long-range jet aircraft for cruising conditions are reported. This category of aircraft is used for intercontinental air traffic, for example, on routes across the North Atlantic. Their share in worldwide civil jet aviation fuel consumption is more than 50%, and they account for about 70% of the global civil jet aircraft NO_x emissions [*Baughcum et al.*, 1996; Gardner et al., 1997]. Both NO and NO_2 emissions are determined in the present investigation. Additional recording of the actual fuel flow and the ambient conditions during each measurement allowed the calculation of the individual emission indices by use of the above "fuel flow" prediction methods. The in-flight measurements and prediction methods will be described, and measured and predicted EI(NO_x) values will be compared.

Additionally, the measured ratios γ =[NO_2]/[NO_x] are used to estimate the corresponding ratio at the engine exit plane, γ_0. Very few measurements of that ratio exist [*Lister et al.*, 1995]. The ICAO emission data set contains the NO_x emission index for surface conditions but gives no information on γ, either for surface or at altitude conditions. The value of γ_0 is important, because it determines the ratio of HNO_2/HNO_3 formed in the first milliseconds [*Arnold et al.*, 1992; *Kärcher et al.*, 1996]. It is of interest also to deduce the NO_x emission index when NO is the only measured NO_x component (as in *Schulte and Schlager* [1996] and in three cases of the present measurement). A simple box model for the near-field plume chemistry and dilution was developed and applied in terms of a parameter study to derive best estimates for γ_0 consistent with the actual observed γ values. Then, in turn, γ_0 was used to calculate EI(NO_x) for the cases in which only NO could be measured.

Instrumentation

For the present measurements a suite of instruments was installed on board the DLR research aircraft *Falcon* (DA-20E). Besides the standard sensors for position, pressure, temperature, humidity, wind, and turbulence [*Bögel and Bau-*

mann, 1991], a UV absorption ozone sensor, and several instruments of participating scientific groups, these were two chemiluminescent NO and NO_x sensors and a non-dispersive infrared CO_2 sensor of DLR [*Schlager et al.,* 1997]. Only data of the latter instruments are used here, and therefore only these instruments will be described.

NO_x Instruments

Figure 1 is a gas flow diagram of the NO/NO_x and CO_2 instruments. NO and NO_x were measured with two identical chemiluminescence NO detectors (detector I and detector II). Detector I (D1) was used to measure the NO volume mixing ratio, and detector II (D2) was combined with a photolytic NO_2-to-NO converter. Detector II thus provides a signal,

$$[NO_c] = [NO] + \epsilon\,[NO_2] \quad (1)$$

which is the sum of the ambient [NO] plus the fraction ϵ of NO_2 that is converted to NO in the photolytic converter. Here, ϵ is the conversion efficiency of the converter. $[NO_x]$ can thus be determined by

$$[NO_x] = [NO] + \epsilon^{-1}([NO_c] - [NO]) \quad (2)$$

(square brackets denote volume mixing ratios). Both instruments are of the type described by *Drummond et al.* [1985].

The NO instruments are equipped with a prereaction chamber for cross-sensitivity determination and zero signal recording. Ambient air is sampled via a Teflon line from a sampling inlet situated above the aircraft mixing layer outside the aircraft fuselage. Sample airflow is driven by a rotary pump connected to the outlets of the detectors. After passing through a first restrictor nozzle the sample air is kept at constant pressure of 120 hPa by removing excess air with a second rotary pump through a pressure-controlled valve (PV). The sample air is then split into two air streams, one leading to detector I and the other to the photolytic converter (PC) which is combined with detector II. In the converter the sample air is irradiated by a Xenon UV lamp for photolytic dissociation of NO_2 to NO. An additional restrictor nozzle at the entrance of each detector, in combination with the constant pressure behind the first nozzle, provides a constant sample gas flow of 3 L/min (STP) and a constant pressure of 35 hPa within both detectors for a wide range of ambient pressures, allowing instrument operation from sea level to the lower stratosphere. For preflight and postflight calibration the NO instruments were supplied with sample air containing known NO concentrations. These were prepared by dynamical gas dilution of a NO/N_2 standard with zero air. The NO/N_2 standard was supplied by BOC Gase GmbH, Stuttgart with a certified accuracy of 2%. Additionally, it is checked from time to time by the Bavarian Environmental Protection Agency (LfU, München) to detect possible degradations of the standard mixture over longer time periods. The overall instrument error, consisting of the error of the dilution system, the error of the NO/N_2 standard mixture, and sensitivity fluctuations of the instrument itself, is 6% for the high [NO] concentrations encountered during the present measurements. The efficiency of the converter for photolytic conversion of NO_2 to NO was determined by supplying known $[NO_2]$ produced by gas phase titration of a NO calibration gas mixture with ozone, which was analyzed by detector II with converter UV lamp turned on and off. An efficiency of 34% could be achieved with the present converter. The calibration of both detectors was checked during the flights with an in-flight calibration system. Through a three-way valve situated upstream of the first restrictor nozzle within the sampling line, both detectors could be supplied with calibration gas of a fixed NO volume mixing ratio or with zero air provided by an air purifier (AP).

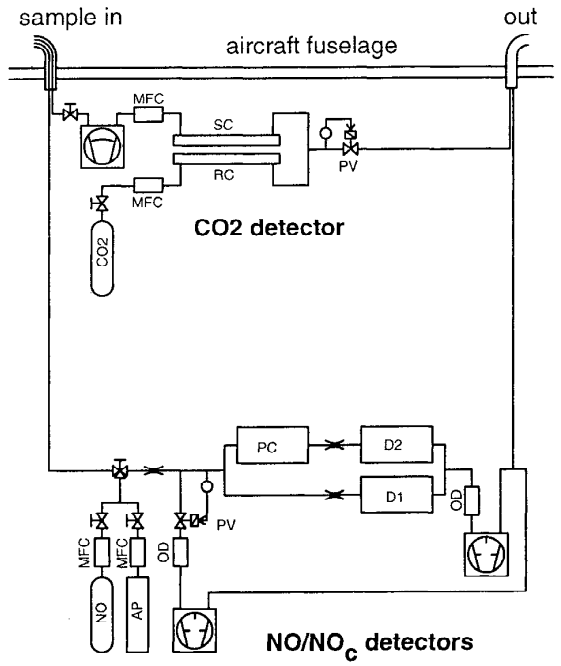

Figure 1. Gas flow diagram the NO-, NO_c- and CO_2 sensors (for description see text). MFC, mass flow controller; SC, sample gas cuvette; RC, reference gas cuvette; PV, pressure-controlled valve; CO2, CO_2 reference gas bottle; NO, NO standard bottle; AP, air purifier; OD, ozone destroyer; PC, photolytic converter; and D1 and D2, NO detectors I and II.

A PC is used to control both instruments and sample the instruments' output via a serial interface (RS-232). The sampling rate was 1 Hz. The response times are about 1 s for the NO measurement and about 3 s for the NO_c measurement.

CO_2 Instrument

A differential nondispersive infrared (NDIR) instrument was used for the present CO_2 measurements, as depicted in Figure 1. It consists of two parallel glass cuvettes, an infrared source, and a pneumatic infrared detector. One cuvette (SC) is supplied with sample air via a Teflon sampling tube from outside the aircraft mixing layer. Before being passed to the instrument the sample air is compressed to 1.1 atm by a diaphragm pump. A constant sample gas flow of 2 L/min (STP) is maintained by a mass flow controller (MFC) behind the pump in the sampling inlet line. The pressure is kept constant by a pressure-controlled valve (PV)

Table 1. Parameters of Individual Interceptions

Case	Aircraft	Engines	Departure	Destination	Day	UTC	N Longitude,	W Latitude,	FL, m	FF, t/h	Ma
1	B747-400	4 GE CF6-80C2B1F	Mexico City	Amsterdam	Nov. 13, 1994	1457	50°40′	10°30′	11278	8.4	0.84
2	B747-100	4 P&W JT9D-7A	Paris	New York	June 30, 1995	1328	51°20′	11°30′	9937	13.6	0.77
3	B747-100	4 P&W JT9D-7A	London	Washington	June 30, 1995	1355	53°00′	14°30′	9144	12	0.81
4	B747-200B	4 GE CF6-50E2	Rome	New York	June 30, 1995	1422	51°45′	14°30′	10668	12	0.85
5	B747-200B	4 P&W JT9D-7J	London	Washington	July 3, 1995	1346	54°15′	11°40′	10058	13.0	0.85
6	DC10-30	3 GE CF6-50C	Los Angeles	Paris	July 3, 1995	1426	52°00′	11°30′	10058	7.4	0.83
7	B747-200B	4 P&W JT9D-7J	London	New York	July 3, 1995	1444	51°15′	13°00′	10058	12.8	0.84
8	B747-100	4 P&W JT9D-7A	London	New York	July 3, 1995	1532	51°05′	14°00′	10058	16.8 (11.3)	0.85
9	B747-200B	4 GE CF6-50E2	New York	Rome	July 5, 1995	0247	52°10′	11°30′	10668	10.4	0.84
10	A340-300	4 G/S CFM56-5C2	Miami	Frankfurt	July 5, 1995	0325	51°45′	9°15′	10668	6.28	0.83

UTC, time of day at start of interception; N Latitude: northern latitude of interception; W Longitude, western longitude of interception; FL, flight level (pressure altitude); FF, fuel flow (the number of decimals reflects the precision of the figures reported by the pilot of intercepted aircraft, the number in parantheses represents an assumed typical value for case 8); and Ma, Mach number.

at the instruments exit. The second cuvette (RC) is flushed with a reference mixture of 380 parts per million by volume (ppmv) CO_2 in dry air at 0.075 L/min (STP). It is supplied by a gas bottle via a MFC and kept at the same pressure as the sample cuvette. Radiation from an IR source passes through both cuvettes via a filter to permit only radiation in the 4.3 μm band of CO_2 to reach the pneumatic infrared detector. A chopper wheel situated between filter and detector switches between radiation from the sample gas cuvette and the reference gas cuvette. The difference between both signals is a measure for the sample gas CO_2 volume mixing ratio. For calibration of the instrument, three different preprepared CO_2/air mixtures covering the instrument range ($[CO_2]_{ref} \pm 50$ ppmv) are used. The reference gas and calibration gas mixtures were supplied by Messer Griesheim GmbH, Sondergasewerk, Duisburg, and are certified to an accuracy of 0.5%. The precision of the instrument is 2%, concerning $[CO_2]$ increases above background values.

The instrument analog output was sampled with 10 Hz over an AD converter and recorded on a PC. The instrument response time is about 1 s.

Measurements

The measurements were made in November 1994 and in June/July 1995 as part of the "Pollution From Aircraft Emissions in the North Atlantic Flight Corridor (POLINAT)" project. The prime goal of POLINAT is to look for measurable and distinguishable effects of subsonic air traffic emissions on the chemical composition and physical state of the upper troposphere/lower stratosphere in the vicinity of the North Atlantic flight corridor during heavy traffic load. During the two aircraft campaigns, four of a total 17 flights were dedicated to direct measurements in very young aircraft exhaust plumes (plume ages less than a few minutes) to determine individual emission indices of various trace species for a variety of aircraft/engine combinations under cruising conditions. Seven individual chasings of specific source aircraft could be carried out, covering six different aircraft/engine combinations and aircraft and engine types from three different aircraft manufacturers and three different engine manufacturers. Three additional aircraft were followed but without NO_c measurement. Table 1 summarizes the aircraft-related parameters of the seven chasings with complete data and of the three cases in which no NO_c was available. Table 2 lists the corresponding atmospheric parameters.

Chasing Procedure

All aircraft chasings reported here took place within the Shannon Radar Control Area, depicted in Figure 2. Those parts of the *Falcon* flight tracks where plume measurements were carried out are also shown. Eastbound as well as westbound source aircraft were chased. During all flights, some members of the POLINAT team were present at the Shannon air traffic control (ATC) center. In collaboration with ATC, suitable source aircraft were chosen that were within reach of the *Falcon* in sufficiently short time to allow for a chasing of several minutes before the source aircraft left the control

Table 2. Parameters Characterizing Ambient Air During Individual Interceptions

Case	p, hPa	T, °C	[H_2O], ppmv	[O_3], ppbv	$j(NO_2)$, 1/s	τ, s
1	216.6	-58	40-45	41 ± 4	0.698E-2	82
2	266.9	-48	50-60	105 ± 19	0.117E-1	68
3	300.9	-42	50-55	118 ± 13	0.116E-1	60
4	238.4	-53	40-50	97 ± 14	0.116E-1	86
5	262.0	-47	60-70	73 ± 3	0.116E-1	125
6	262.0	-47	70-85	76 ± 4	0.116E-1	87
7	262.0	-47	80-100	74 ± 5	0.115E-1	103
8	262.0	-47	70-90	71 ± 4	0.114E-1	82
9	238.4	-52	60-70	55 ± 6	0.0	87
10	238.4	-52	60-80	57 ± 5	0.0	102

p, static pressure; T, air temperature at flight level; [H_2O], volume mixing ratio of water; [O_3], ozone volume mixing ratio as measured with on-board ozone sensor; $j(NO_2)$, NO_2 photolysis rate calculated for clear sky after *Ruggaber et al.* [1994], for day, UTC and flight level according to Table 1; and τ, reference plume age used for modelling of $\gamma = \Delta[NO_2]/\Delta[NO_x]$.

zone. ATC directed both aircraft until visible contact was established. After that time the *Falcon* pilot received permission to enter the exhaust trail of the chased aircraft when he considered it safe enough, typically at a distance of 10 km behind the source aircraft. During the measurements the source aircraft pilot was asked to report his actual fuel flow to allow for later calculation of NO_x emission indices. Additional parameters collected at the ATC center during the measurements were aircraft identification for later determination of the exact aircraft and engine types, departure and destination airport, ground speed (GS) and pressure altitude of *Falcon* and source aircraft, and distance between *Falcon* and source aircraft. The latter three quantities were recorded by monitoring the radar display screen with a video camera. In one case (case 10, Table 1) in addition, high-accuracy on-board recorded fuel flow and various aircraft/engine data were provided by the operating airline. The ground speed (GS) was used to calculate the true airspeed (TAS) and the Mach number (Ma), taking into account the actual wind vector and the temperature as recorded on board the *Falcon*. From TAS and distance between *Falcon* and source aircraft the plume age τ during the measurement could be calculated. All parameters necessary to infer the actual emission indices from the corresponding ICAO data sheet can be found in Tables 1 and 2. Figure 3 shows data collected during chasing of a A340-300 with four G/S CMF56-5C2 engines (case 10 from Table 1). The data recorded on board the *Falcon* are presented as solid lines, while the data collected at the ATC center are given as symbols. NO, NO_c, and CO_2 volume mixing ratios are shown together with temperature, altitude, ground speed, and distance. [NO] and [NO_c] are not distinguishable from each other in this presentation, because both signals were very similar. During the plume measurements the occurrence of turbulence was clearly noticeable, which was not the case during periods outside any aircraft plume. It was most pronounced where the very high peak values of [NO], [NO_c], and [CO_2] occurred, leading to extremely exceptional flight attitudes of the *Falcon*. This was the case when the *Falcon* directly penetrated one of the trailing vortices of the source aircraft. Normally, the *Falcon* pilot tried to avoid the vortices, maintaining an altitude slightly above them, but as a result of unpredictable motions of the vortices in the plane perpendicular to the source aircraft flight track, this tactic was not always possible. Three vortex penetrations can clearly be distinguished in Figure 3. Most of the engine exhaust data were collected in the secondary plume above the vortices, which is produced by ex-

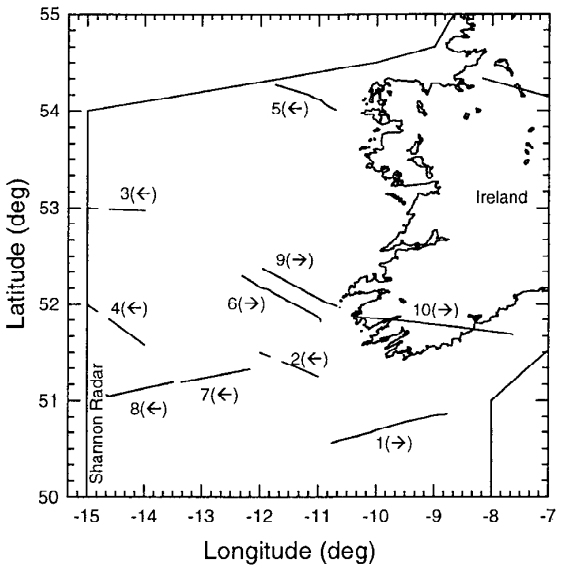

Figure 2. Measuring area for the [NO_x] measurements carried out during POLINAT. The border of the Shannon radar control zone is indicated, and those sections of the *Falcon* flight tracks where plume measurements took place are plotted and marked according to the numbering in Table 1. The arrows indicate the flight direction (right arrow, eastbound; left arrow, westbound). Dashed lines represent cases in which no position was recorded in flight and the location of the chasing was determined from the video record of the ATC radar screen.

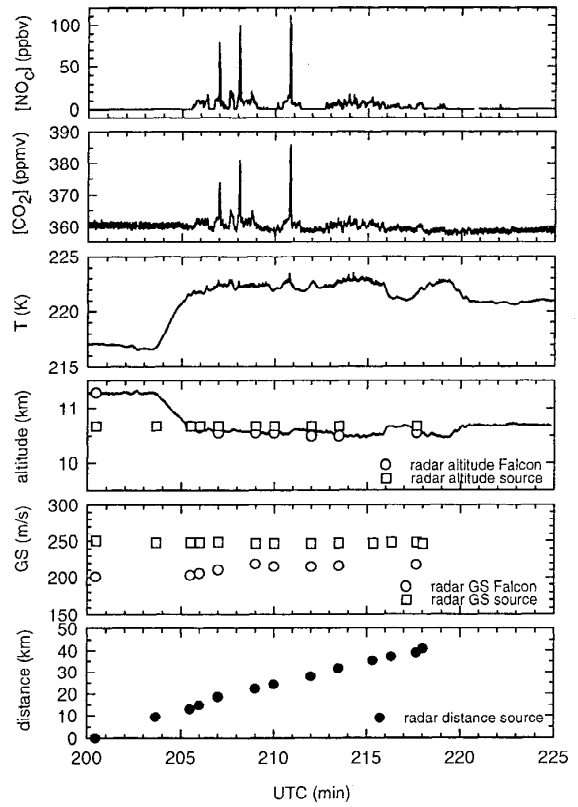

Figure 3. Example of data recorded during a plume measurement (Case 10 of Table 1, A340-300 with G/S CFM56-5C2 engines). Solid lines present data recorded on board *Falcon*; symbols are data collected from the radar screen display at the Shannon ATC center. Shown in descending order as a function of time are [NO] and [NO_c] (not distinguishable from each other because data differed only slightly), [CO_2], temperature T, altitude h, ground speed GS, and relative distance of *Falcon* and target.

haust gas detrainment from the downward traveling vortex pair [*Gerz and Ehret,* 1996].

Data Reduction

To obtain the aircraft-produced [NO_x] and [CO_2], we have to substract the contributions of ambient air in the samples. To distinguish air samples being influenced by aircraft exhaust from completely undisturbed background air, a threshold NO value of 100 to 250 parts per trillion by volume (pptv) was chosen, depending on the actual NO background level and its variation observed during the individual flight sections outside the aircraft plume. For periods during a chasing in which [NO] exceeded that threshold value, all three signals ([NO], [NO_c] and [CO_2]) were considered to be influenced by aircraft emissions. These periods were cut out of the data set, and the remaining background data points were smoothed by calculating 10 s mean values. These data are then used to reconstruct a complete background signal by linear interpolation between the resulting 10 s mean values. This smoothed background signal was substracted from the corresponding original signal. Figure 4 shows the resulting Δ[NO], Δ[NO_c], and Δ[CO_2] signals for case 10 (Table 1).

NO_x Emission Indices

Measured NO_x Emission Indices

From [NO], [NO_c], and [CO_2] the emission index of NO_x can be obtained by [e.g., *Schulte and Schlager,* 1996]

$$\mathrm{EI}(\mathrm{NO}_x) = \mathrm{EI}(\mathrm{CO}_2)\,\frac{46}{44}\,\frac{\Delta[\mathrm{NO}_x]}{\Delta[\mathrm{CO}_2]} \quad . \tag{3}$$

Here, EI(CO_2) is the CO_2 emission index, and 46 and 44 are the mole masses of NO_2 and CO_2, respectively. Δ[NO_x] is calculated according to equation (2). EI(CO_2) is known with high accuracy (3153 $\pm$ 15 g/kg) [*Schulte and Schlager,* 1996]. Thus

$$\mathrm{EI}(\mathrm{NO}_x) = 3296\,\frac{\Delta[\mathrm{NO}] + \epsilon^{-1}(\Delta[\mathrm{NO}_c] - \Delta[\mathrm{NO}])}{\Delta[\mathrm{CO}_2]} \tag{4}$$

in g/kg. For the present EI determinations the volume mixing ratio expressions in equation (4), Δ[CO_2], Δ[NO], and Δ[NO_c], were replaced by the corresponding integrals, with integration interval starting and ending in regions where all three signals were zero. This method was necessary because all three signals are subject to different time delays due to different length of sampling lines. Additionally, all three instruments have different reaction time constants because of unavoidable mixing in the instruments' inner volumes (reaction, zeroing, and photolysis chambers in the NO and NO_c

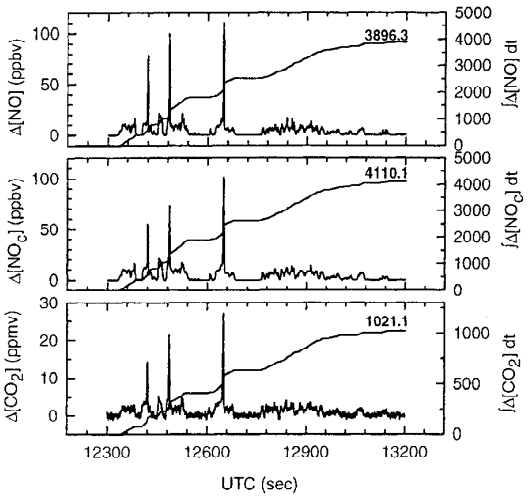

Figure 4. Time series of [NO], [NO_c], and [CO_2] from example 10 (see Table 1 and Figure 2) after background subtraction (left axis). Shown is the time interval over which the integration was taken. The monotonically growing lines show the respective time integral over the data (right axis). The numbers at the end of the integral curves indicate the integral values at the end of the interval, which are used for the emission index determination.

instruments and cuvettes in the CO_2 instrument). Therefore equation (4) cannot be evaluated point by point. However, if integration is carried out under the above constraints, it can be shown that equation (4) is still valid and no exact knowledge of the time constants is necessary. This is true even when the ratio $\gamma = \Delta[NO_2]/\Delta[NO_x]$ changes with time, as long as NO_x can be considered a conservative tracer. In Figure 4 the integral over each signal is shown for the range of data used for emission index determination in case 10. The numbers at the end of each curve indicate the total integral value used in equation (4). The results for all cases from Table 1 are listed in Table 3 together with some parameters characterizing the quality of the data. The errors of the measured values range from 10.3% to 11.8%. They include the calibrational error of the instruments, the statistical error of the NO detector count rates (which is very small as a result of high intensity signals and integration), and the noise of the $[CO_2]$ background signal.

Also given in Table 3 are the observed values of γ, again calculated by using integrals instead of single values. Chemical transformation of NO into NO_2 by reaction with ozone and reformation of NO by NO_2 photolysis occurs on a timescale comparable to the integration time period, and therefore γ cannot be assumed constant over the integration period. Therefore the tabulated numbers instead represent mean values of γ for plume ages between about 50 s and 150 s. The considerable difference between γ values for cases 1 and 5-8 in comparison with cases 9 and 10 is due to the fact that cases 9 and 10 were measured during nighttime, with no NO_2 photolysis counteracting NO_2 buildup by the $NO-O_3$ reaction.

EI(NO_x) Prediction Methods

The two fuel flow based emission index prediction methods used in the present work (Boeing method 2 [*Baughcum et al.*, 1996] and DLR fuel flow method [*Deidewig et al.*, 1996]) are quite similar. Given a specific aircraft/engine combination flying under certain ambient temperature T_a, pressure p_a, and water vapor mixing ratio q_a conditions, the following steps have to be followed:

Step 1: Correction of ICAO data sheet for installation effects (Boeing method only). The ICAO data have been measured for a specific engine on a ground test facility under sea level conditions. They do not account for the aircraft in which the engine is to be installed, nor do they account for the fraction of the engine thrust or energy output consumed by aircraft systems (bleed air). Therefore the fuel flow F column in the ICAO data sheet for the respective engine has to be rescaled to correct for the above installation effects, yielding an installation-corrected fuel flow F_{ic} for that engine when combined with a certain aircraft. The correction is usually less than 5%. The dependency of the sea level or reference NO_x emission index, $EI(NO_x)_{ref}$, from F_{ic} is mostly a simple linear function (on a log-log scale), and EI values for fuel flows other than the four values tabulated in the installation-corrected ICAO data sheet can be easily obtained by linear interpolation.

Table 3. Emission Indices EI(NO_x)

Case	n	$\Delta\tau$, s	$\Delta[NO]_{max}$, ppbv	$\Delta[CO_2]_{max}$, ppmv	EI(NO_x), g/kg			γ
					Measured	DLR	Boeing	
1	53	58-175	57.7	14.9	12.3	9.2	10.8	0.06
2	184	67-83	50.9	8.3	(20.1)	22.0	19.7	(0.12)
3	219	58-93	184.0	25.4	(22.1)	19.9	17.6	(0.15)
4	315	46-102	71.2	10.4	(14.9)	18.3	18.1	(0.10)
5	153	70-130	93.1	12.8	23.7	26.0	23.4	0.09
6	107	75-107	36.8	5.4	19.7	14.7	15.0	0.11
7	269	57-121	222.6	25.0	30.4	25.2	23.0	0.06
8	297	59-105	57.0	7.7	21.0	36.8 (21.4)	31.1 (17.3)	0.07
9	207	61-104	318.5	51.3	17.0	15.8	15.8	0.23
10	576	54-175	110.1	27.1	16.2	15.4	16.2	0.22

n, number of NO data points with $\Delta[NO]$ exceeding 3σ of background noise. $\Delta\tau$, range of plume ages covered during measurement. $\Delta[NO]_{max}$, maximum observed NO increase in plume. $\Delta[CO_2]_{max}$, maximum observed CO_2 increase in plume. Measured, DLR, Boeing, NO_x emission indices derived from measurement and calculated with the DLR fuel flow method and Boeing method 2, respectively. In cases 2, 3, and 4, in which no NO_c could be measured, the tabulated "measured" values are derived by using $\Delta[NO_x] = \Delta[NO]/(1-\gamma)$ in equation (3), with γ estimated by plume model assuming $\gamma_0 = 0.07$; they are given in parantheses. For case 8 the values in parantheses were calculated for an assumed typical fuel flow (see Table 1). γ, NO_2 fraction of engine-produced NO_x at plume age of observation (values in parantheses are obtained from plume model, assuming $\gamma_0 = 0.07$ at engine exit plane).

Step 2: Determination of reference sea level fuel flow from actual fuel flow. For the Boeing method the reference fuel flow for sea level conditions, F_{ref} , is determined from the actual fuel flow at altitude, F_a, by use of the equation

$$F_{ref} = F_a \, \delta_a^{-1} \, \Theta_a^{3.8} \exp(0.2\,\mathrm{Ma}^2) \qquad (5)$$

with $\Theta_a = T_a/T_0$ and $\delta_a = p_a/p_0$. T_a and p_a are the actual ambient temperature and pressure, T_0 and p_0 are the corresponding sea level values (288.15 K and 1013.25 hPa, respectively), and $\exp(0.2\,\mathrm{Ma}^2)$ is an explicit Mach number correction term.

The DLR fuel flow method uses a similar equation:

$$F_{ref} = F_a \, \delta_i^{-1} \, \Theta_i^{-0.5} \qquad (6)$$

with $\Theta_i = T_i/T_0$ and $\delta_i = p_i/p_0$. T_i and p_i are the temperature and pressure at engine air intake, respectively, and are calculated from the ambient values by

$$T_i = T_a\,(1 + 0.2\,\mathrm{Ma}^{0.2}) \qquad (7)$$

$$p_i = p_a\,(1 + 0.2\,\mathrm{Ma}^{0.2})^{3.5} \quad , \qquad (8)$$

thus implicitly applying a Mach number correction.

Step 3: Determination of reference emission index. The reference emission index $\mathrm{EI(NO}_x)_{ref}$ for sea level conditions is obtained from the ICAO data sheet by interpolating for the reference fuel flow F_{ref} given by step 2. For Boeing method 2 the installation-corrected data sheet is used (see step 1).

Step 4: Determination of actual emission index at altitude. With the equation

$$\mathrm{EI(NO}_x) = \mathrm{EI(NO}_x)_{ref} \, \delta^{\alpha} \, \Theta^{\beta} \, H_c \qquad (9)$$

the actual emission index $\mathrm{EI(NO}_x)$ is then inferred from the reference value $\mathrm{EI(NO}_x)_{ref}$ resulting from step 3. Here, δ and Θ are as defined for equations (5) and (6) for the respective method. H_c is a humidity correction factor defined as $H_c = \exp(-19(q - 0.0063))$ with q being the water vapor mixing ratio (mass of water vapor per mass of dry air) at altitude. Here, 0.0063 is the mixing ratio under sea level standard conditions at a relative humidity of 60%). H_c is the same for both methods and covers a range of 1.1263 ± 0.0002 for all H_2O volume mixing ratios listed in Table 2. The exponents are $\alpha = 0.51$ and $\beta = -1.65$ for the Boeing method 2. For the DLR method, $\alpha = 0.4$ and $\beta = 3$ are used. The results of the two methods when the figures from Tables 1 and 2 are used as input parameters are listed in Table 3.

Discussion

Figure 5 shows a comparison of measured and calculated $\mathrm{EI(NO}_x)$. Each data point represents an individual pair of measured value and related prediction. The open circles show the DLR fuel flow method results, and the solid circles show the Boeing method 2 results, in comparison with the measured values. The solid line marks perfect agreement between measurement and prediction.

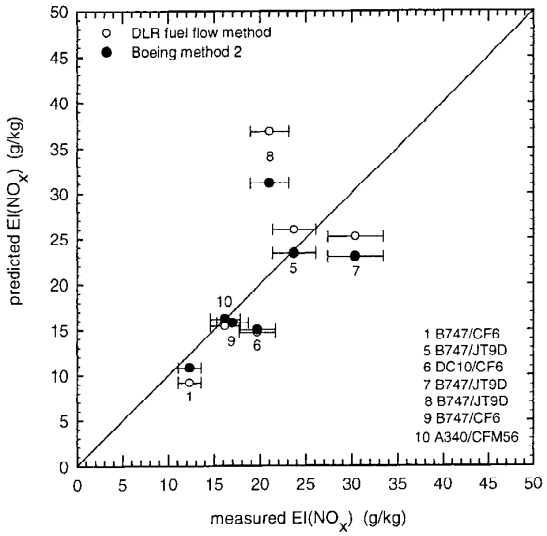

Figure 5. Comparison between measured (horizontal axis) and predicted EI values (vertical axis). The prediction calculations were carried out by using the DLR fuel flow method (open circles) and the Boeing method 2 (solid circles), respectively, as described in the text. The error bars represent the error of the measured EI values. The numbers indicate the source aircraft according to Table 1.

In case 8 an unusually high fuel flow was reported by the source aircraft pilot. Representatives of the airline, when asked later on, confirmed that this value was rather high but not impossible under certain circumstances. However, the values calculated for the reported fuel flow are much higher than the value derived from the measurement. Therefore the calculations were carried out a second time, based on an assumed typical fuel flow for that aircraft/engine combination, yielding a much better agreement with the measured value (Tables 1 and 3, values in parantheses). However, case 8 will be excluded from the following discussion and is only listed for completeness.

The correspondence between predicted and measured values can be expressed in terms of relative deviation of predictions from measurement. We find that the DLR fuel flow method values are lower by 11.7% ± 13.6%, and the Boeing method 2 values by 11.5% ± 10.7% than the measured values. For both methods, half the values are within or close to the 11% uncertainty of the measurement. Very good agreement between measured EI and both predicted values is found for case 10 (Airbus A340-300 with four G/S CFM56-5C2 engines). In this case the fuel flow was very accurately known, because the operator of the aircraft provided the relevant data from the flight data recorder. Both predictions deviate less than 5% from the measured value. Thus it might well be that low precision of the reported fuel flow rates is one reason for the larger differences in the other cases. For example, the Boeing method 2 would lead to a 14% error in predicted EI if the fuel flow were wrong by 10%. Another point to be considered is how representative the ICAO emission indices of a certain engine type are when the ground

tests are carried out mainly on new engines. Any possible variabilities between engines of identical type due to aging or state of maintenance are not accounted for. The existence of such variabilities is indicated by cases 5 and 7. Both were B747-200B aircraft with JT9D-7J engines, investigated during the same flight within 1 hour and under nearly identical atmospheric conditions. Both were westbound, coming from London and heading for New York and Washington, respectively. The only known difference between the two cases is the age of the engine: in case 5 it came into service in 1976, and in case 7 it came into service in 1971. A difference of more than 20% between the measured EI(NO_x) of the two cases was observed. This finding suggests that the age and/or state of maintenance of an engine may be important and that the emission index might change with time on duty.

Disregarding the measured values, we can compare the predicted values with each other by relating the prediction values to the respective mean from both methods. This comparison reveals 0.6% ± 9.8%, indicating that both methods disagree up to about 10% in individual cases but agree quite well on the average.

$\Delta[NO_2]/\Delta[NO_x]$ Ratio at Engine Exit Plane

In young exhaust plumes, i.e., at plume ages small in comparison with the time required to reach photochemical equilibrium between NO, NO_2, and ozone, γ can be used to infer its initial value γ_0 at the engine exit plane with a proper plume chemistry model. For this purpose a simple box model was developed, which simulates the plume chemistry in terms of the three reactions

$$NO + O_3 \longrightarrow NO_2 + O_2 \quad (10)$$

$$NO_2 + h\nu \longrightarrow NO + O \quad (11)$$

$$O_2 + O + M \longrightarrow O_3 + M \quad (12)$$

These reactions determine γ in young exhaust plumes. Our plume model solves for the abundance rates of NO, NO_2, O_3, and O. It describes mixing with ambient air by a mixing rate $d(\ln N)/dt$, where $N = \max(70, N_0(t/s)^{0.8})$ is the assumed dilution factor, i.e., the amount of plume air mass that mixes with the exhaust gases from one unit of fuel mass [*Schumann*, 1996]. The limit $N = 70$ is the dilution at the engine core exit corresponding to typical air/fuel mass ratios of modern engines at cruise. The value N_0 (about 3500) is determined such that the model matches the maximum measured $[CO_2]$ increase above ambient values at a reference plume age τ,

$$\Delta[CO_2](\tau) = \frac{EI(CO_2)}{N(\tau)} \frac{28.96}{44} \quad (13)$$

where 28.96 and 44 are the molar masses of air and CO_2, respectively. The reference plume age τ was defined as the plume age at which the $\Delta[CO_2]$ peak value occurred. This was generally at or close to plume age when the integral over $\Delta[CO_2]$ reaches half the final value (see Figure 4). The corresponding reference τ values are listed in Table 2.

Initial values prescribe

$$\Delta[NO_x]_{\tau=0} = \frac{EI(NO_x)}{N_{\tau=0}} \frac{28.96}{46} \quad (14)$$

with 46 being the molar mass of NO_2, measured emission indices EI(NO_x) and $\Delta[NO_2]_0 = \gamma_0\Delta[NO_x]$, $\Delta[NO]_0 = (1 - \gamma_0)\Delta[NO_x]$, and $\Delta[O_3] = 0$. Here, γ_0 is a model parameter. The plume excess temperature at any time t is computed from

$$\Delta T(t) = \min\left(\frac{(1-\eta)Q}{c_p N(t)}, \frac{0.6\,Q}{c_p N(0)}\right) , \quad (15)$$

where $Q = 43$ MJ kg^{-1}, $c_p = 1004$ J kg^{-1} K^{-1}, and $\eta = 0.3$ are the specific combustion heat, heat capacity, and overall propulsion efficiency, respectively [*Schumann*, 1996].

For small times the temperature is limited, because the core exit carries only about 60% of the exhaust heat, while the remainder leaves the engine with the bypass air or is used to propel the aircraft. The exhaust gases in the plume are assumed to mix with ambient air having O_3 concentrations as measured and with 100 pptv ambient nitrogen oxides with the $[NO_2]/[NO_x]$ ratio in photochemical equilibrium. The reaction rate coefficient k for NO + O_3 is taken from *Atkinson et al.* [1996]; the photolysis rate coefficient $j(NO_2)$ is computed for clear sky by using the model of *Ruggaber et al.* [1994] and then enlarged by a factor of 2 to account for enhancements above cloud decks [*Kelley et al.*, 1995; *Vilà-Guerau de Arellano et al.*, 1994] over which the plume measurements took place. The j values used are 0.014 s^{-1} for case 1 and 0.023 s^{-1} for all other daytime cases.

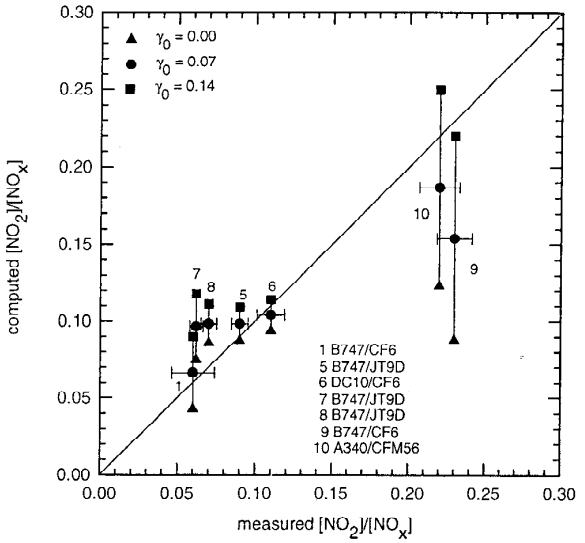

Figure 6. Comparison of computed ratios $\gamma = [NO_2]/[NO_x]$ with γ values derived from measurement in the exhaust plume for daytime cases 1 and 5-8 and nighttime cases 9 and 10. The vertical bars on the computed values indicate the range of actual $\gamma(\tau)$ values found for initial values of 0, 0.07, and 0.14 for $\gamma_0 = \gamma(\tau - 0)$ at the engine exit plane. The horizontal bars represent the errors of γ derived from the measurements.

Figure 6 shows the computed $\gamma(\tau)$ ratios in the plumes of age τ versus the ratio of values measured during the plume chasings. The diagram exhibits results for initial values of γ_0 of 0.00, 0.07, and 0.14. The horizontal error bars represent the errors in γ as determined from the measurement. They are rather low (less than 8% except for case 1), because only the error of the conversion efficiency (about 6%) and statistical errors have to be taken into account. Statistical errors lead to a higher error of 23% only in case 1. Calibrational errors all act in the same direction on [NO] and [NO_c] and thus do not influence the ratio γ.

We see that the computed results match the measured values reasonably well. The measured values are most accurate for the nighttime cases 9 and 10 because of largest NO_2 fractions and longest integration times. The sensitivity of the computed results to γ_0 is also largest for the nighttime cases, while it is small for the daytime cases 1 and 5-8, which are already close to photochemical equilibrium. The computed daytime results agree best with the measured values for small values of $\gamma_0 < 0.07$, while the nighttime results 9 and 10 agree best for γ_0 of 0.1 to 0.15. One cannot exclude that the γ values differ from engine to engine. But model uncertainties may also be responsible for the apparent difference between the various measurements. The smallest value of $\gamma(\tau)$, and hence the largest value of γ_0, is obtained for large photolysis rates and small reaction rates $k\cdot[O_3]$). Also, photolysis of HNO_3 may contribute to additional NO_2 formation. For this reason, we performed a parameter study and evaluated the same cases with more complex chemistry models, including the cycles used by *Louisnard et al.* [1995] and *Kärcher et al.* [1996]. The parameter study considered factor of 3 variations in the dilution fractor N_0, $\pm 50\%$ changes in the photolysis rates, reductions of the reaction rate coefficient k by 30%, and variations in plume temperature (with and without ΔT).

The computations suggest that the engine exit values of $\gamma = [NO_2]/[NO_x]$ for all seven measured cases was in the range 0 to 0.15 as a best estimate, possibly extending up to 0.25 if all uncertainties are taken into account. This finding is consistent with γ_0 values of the order of 0.03 ± 0.02 measured in altitude test chambers [*Lister et al.*, 1995]. Such small values imply HNO_3/HNO_2 ratios below 0.5 in young plumes [*Kärcher et al.*, 1996]. Some measurements [*Arnold et al.*, 1994; F. Arnold, personal communication, 1996] indicate larger values for this ratio of the order of 1. Hence the model deductions have to be taken with care.

Computations of γ at the time of the measurements can now be used to estimate the emission index for NO_x when only NO was measured: the effective emission index of NO_x is a factor of $1/(1-\gamma(\tau))$ larger than the emission index $EI(NO) = 3296\Delta[NO]/\Delta[CO_2]$, deduced from NO alone. For an assumed initial value $\gamma_0 = 0.07$ this correction was calculated for plume cases 2, 3, and 4 (Table 1). The resulting γ and EI values are listed in Table 3 (values in parantheses).

The same kind of correction can also be applied to the EI(NO) values given by *Schulte and Schlager* [1996]. As a result the effective emission indices are obtained from the NO-based lower limit values by multiplication with factors

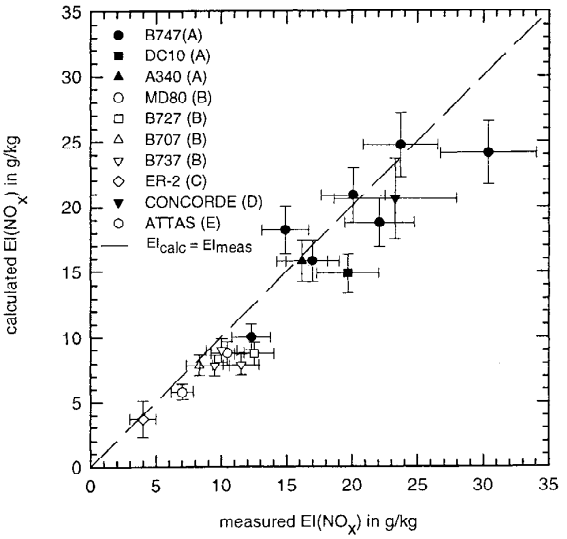

Figure 7. Overview of the available in situ measurements of jet aircraft engine NO_x emission indices in comparison with the corresponding predicted values. For details on the respective measurement circumstances, the engine types, and the prediction method used, see the references: A this study; B *Schulte and Schlager* [1996]; C *Fahey et al.* [1995a]; D *Fahey et al.* [1995b]; and E *Haschberger and Lindermeir* [1996].

1.08, 1.10, 1.28, 1.19, 1.32, and 1.32, for the list of six aircraft they considered. For $\gamma_0 = 0$ the factors are 1.06, 1.08, 1.27, 1.16, 1.28, and 1.31. The differences are smaller the closer γ is to photochemical equilibrium. The largest factor (1.32) changes between 1.23 and 1.43 when j is varied by $\pm 50\%$. With these corrections, all emission indices measured for these 6 cases exceed the predicted values presented by *Schulte and Schlager* [1996]. We note that the neglect of HNO_2 and HNO_3 formed in the exhaust plume causes a further underestimate of the actual NO_x emission index, but probably only by a few percent.

In Figure 7 the corrected EI values for cases 2, 3, and 4 of the present study and for the six values from *Schulte and Schlager* [1996] are compared with the respective mean of the predictions resulting from the two different fuel flow methods. Additionally, the EI values derived directly from the measurements in the present work and the data of comparable studies concerning the NASA ER-2 aircraft [*Fahey et al.*, 1995a], the Concorde [*Fahey et al.*,1995a], and the DLR ATTAS (VFW-614) aircraft [*Haschberger and Lindermeir*, 1996] are included. When no error for the predicted values was given, a value of 10% was applied. A linear regression over all data points confirms the above finding that the predictions underestimate the NO_x emission indices by about 11%.

Summary and Conclusions

Using the DLR research aircraft *Falcon*, we have carried out first in situ measurements of NO_x emission indices of commercial long-range jet airliners at cruising altitude by

simultaneous observations of $[NO_x]$ and $[CO_2]$ increases in the near-field exhaust plumes of seven specific source aircraft. The aircraft/engine combinations investigated are representative of those typically serving on long distance routes like the North Atlantic flight corridor and contribute to approximately half the NO_x produced by commercial jet aircraft. At plume ages between 50 s and 150 s, maximum observed exhaust gas enhancements of 319 ppbv and 51 ppmv for $\Delta[NO_x]$ and $\Delta[CO_2]$, respectively, relative to ambient values, were found. Measured emission indices ranged from 12.3 g/kg to 30.4 g/kg. Also, auxiliary data, such as actual source aircraft fuel flow, Mach number, atmospheric pressure, temperature, and humidity, were collected to allow independent calculation of the individual NO_x emission indices. Thereby a test of the emission index prediction methods applied for construction of recent NO_x emission inventories (Boeing method 2 in [*Baughcum et al.*, 1996]; DLR method in [DLR, unpublished emission inventory, 1997] and [ECAC/ANCAT & EC Working Group, unpublished emission inventory, 1997]) was possible for the first time. When one of the seven cases (case 8), which seems to have an unreasonably high (although not impossible) reported fuel flow, is disregarded, the calculated emission indices from both methods underestimated the measured values on average by 12%, with a maximum deviation of 25%. Half the predictions lie within or close to the error limits of the measurements (about 11%). Thus the present study gives some confidence in the prediction abilities of both methods, though, the number of single cases studied here is too small to state this as a general conclusion.

The larger deviations in some cases are probably caused by factors not inherent to the prediction methods themselves, but rather in uncertainties of their input parameters: (1) low accuracy of the reported fuel flow rates in some of the cases, as indicated by the excellent agreement in one case in which fuel flow was very accurately known, (2) possible deviation of the ICAO certification EI values, which are key input parameters in both prediction methods, from ensemble mean EI values, and (3) possible variability of emission indices among engines of the same type and for identical conditions (see cases 5 and 7), for example, due to aging effects or differences in state of maintenance.

When compared only with each other, the results of both methods differed by at most 16% in individual cases, and the average difference was only 0.6%. Thus the cases studied here give no indication that the use of different prediction methods can account for any differences in the emission inventories [*Baughcum et al.*, 1996]; DLR, unpublished emission inventory, 1997; ECAC/ANCAT & EC Working Group, unpublished emission inventory, 1997]].

The ratios $\gamma = [NO_2]/[NO_x]$ determined from the measurement range between 0.06 and 0.23. From these data and a plume chemistry model, best estimate initial values γ_0 between 0 and 0.15 were deduced. Because of large uncertainties in the photolysis rates, γ_0 values of up to 0.25 cannot be excluded. According to these findings, an assumed typical engine exit value of $\gamma_0 = 0.07$ was applied to calculate the actual γ at time of measurement for those cases in which only NO was measured and hence only EI(NO) was known, i.e. for cases 2, 3, and 4, reported in this work, and for the six cases reported by *Schulte and Schlager* [1996]. These calculated γ values allowed correction of the EI(NO) values derived from these nine cases to yield effective $EI(NO_x)$ values. Correction factors ranging from 1.1 to 1.3 were found.

With this model based correction, the emission indices derived from the measurements are slightly larger than the corresponding predictions. The difference is of the same order as the above 12% average difference between measurement and prediction. However, this difference is at the limit of being significant. Overall, the fuel flow based correlations approximate the measured values within the range of model input and measurement uncertainties.

Acknowledgments. The authors are very grateful to the DLR pilots and the Shannon air traffic controllers for their excellent and efficient work. They also wish to thank C. Feigl and R. Marquardt for their help in acquiring this data set. Engine performance data were kindly provided by Lufthansa. This work was supported by the Commission of the European Communities within the POLINAT project under contract EV5V-CT93-0310 (DG 12 DTEE).

References

Arnold, F., J. Scheid, T. Stilp, H. Schlager, and M. E. Reinhardt, Measurements of jet aircraft emissions at cruise altitude, 1, The odd nitrogen gases NO, NO_2, HNO_2 and HNO_3, *Geophys. Res. Lett., 19*, 2421-2424, 1992.

Arnold, F., J. Schneider, M. Klemm, J. Scheid, T. Stilp, H. Schlager, P. Schulte, and M. E. Reinhardt, Mass spectrometer measurements of SO_2 and reactive nitrogen gases in the exhaust plumes of commercial jet airliners at cruise altitude, *Rep. DLR Mitt. 94-06*, pp. 323-328, Dtsch. Forsch. Anstalt für Luft- und Raumfahrt, Köln, 1994.

Atkinson, R., D. L. Baulch, R. A. Cox, R. F. Hampson Jr., J. A. Kerr, M. J. Rossi, and J. Troe, Evaluated kinetic and photochemical data for atmospheric chemistry: Supplement V., *Atmos. Environ., 30*, 3903-3904, 1996.

Baughcum, S. L., T. G. Tritz, S. C. Henderson, and D. C. Pickett, Scheduled civil air traffic emission inventories for 1992: Database development and analysis, *NASA Contract. Rep. 4700*, 72 pp., 1996.

Beck, J. P., C. E. Reeves, A. A. M. de Leeuw, and S. A. Penkett, The effects of aircraft emissions on tropospheric ozone in the northern hemisphere, *Atmos. Environ., 26A*, 17-29, 1992.

Bögel, W., and R. Baumann, Test and calibration of the DLR *Falcon* wind measuring system by maneuvers, *J. Atmos. Oceanic Technol., 8*, 5-18, 1991.

Brasseur, G. P., J.-F. Müller, and C. Garnier, Atmospheric impact of NO_x emissions by subsonic aircraft: A three-dimensional model study, *J. Geophys. Res., 101*, 1423-1428, 1996.

Danilin, M. Y., B. C. Krüger, and A. Ebel, Short-term atmospheric effects of high-altitude aircraft emissions, *Ann. Geophys., 10*, 904-911, 1992.

Deidewig, F., A. Döpelheuer, and M. Lecht, Methods to assess aircraft engine emissions in flight, paper presented at 20th Congress of the International Council of Aronautical Sciences, Sorrento, Italy, Sept. 8-13, 1996.

Drummond, J. W., A. Volz, and D. H. Ehhalt, An optimized chemiluminescence detector for tropospheric NO measurements, *J. Atmos. Chem., 2*, 287-306, 1985.

Ehhalt, D. H., F. Rohrer, and A. Wahner, Sources and distribution of NO_x in the upper troposphere at northern mid-latitudes, *J. Geophys. Res., 97*, 3725-3738, 1992.

Fahey, D. W., et al., In situ observations in aircraft exhaust plumes in the lower stratophere at mid-latitudes, *J. Geophys. Res., 100*, 3065-3074, 1995a.

Fahey, D. W., et al., Emission measurements of the Concorde su-

personic aircraft in the lower stratosphere, *Science, 270*, 70-74, 1995b.

Gardner, R. M., et al., The ANCAT/EC global inventory of NO_x emissions from aircraft, *Atmos. Environ., 31*, 1751-1766, 1997.

Gerz, T., and T. Ehret, Wake dynamics and exhaust distribution behind cruising aircraft, *AGARD Conf. Proc., CP-584*, 35.1-35.12, 1996.

Haschberger, P., and E. Lindermeir, Spectrometric inflight measurement of aircraft exhaust emissions: First results of the June 1995 campaign, *J. Geophys. Res., 101*, 25,995-26,006, 1996.

International Civil Aviation Organisation (ICAO), ICAO engine exhaust emission databank, 1st ed., *ICAO Doc. 9646-AN/934*, Montreal, 1995.

Johnson, C., J. Henshaw, and G. McInnes, Impact of aircraft and surface emissions of nitrogen oxides on tropospheric ozone and global warming, *Nature, 355*, 69-71, 1992.

Kärcher, B., M. M. Hirschberg, and P. Fabian, Small-scale chemical evolution of aircraft exhaust species at cruising altitude, *J. Geophys. Res., 101*, 15,169-15,190, 1996.

Kelley, P., R. R. Dickerson, W. T. Luke, and G. L. Kok, Rate of NO_2 photolysis from the surface to 7.6 km altitude in clear-sky and clouds, *Geophys. Res. Lett., 22*, 2621-2624, 1995.

Köhler, I., R. Sausen, and R. Reinberger, Contributions of aircraft emissions to the atmospheric NO_x content, *Atmos. Environ., 31*, 1801-1818, 1997.

Lister, D. H., et al., Engine exhaust emissions, in *AERONOX: The Impact of NO_x Emissions From Aircraft Upon the Atmosphere at Flight Altitudes 8-15 km, Publ. EUR 16209 EN*, pp. 33-127, Off. for Publ. of the Eur. Comm., Brussels, Belgium, 1995.

Louisnard, N., et al., Physics and chemistry in the aircraft wake, in *AERONOX: The Impact of NO_x Emissions From Aircraft Upon the Atmosphere at Flight Altitudes 8-15 km, Publ. EUR 16209 EN*, pp. 195-309, Off. for Publ. of the Eur. Comm., Brussels, Belgium, 1995.

McInnes, G., and C. T. Walker, The global distribution of aircraft air pollutant emissions, *Rep. LR 872 (AP)*, 39 pp., Warren Spring Lab., Stevenage, England, 1992.

Ruggaber, A., R. Dlugi, and T. Nakajima, Modelling radiation quantities and photolysis frequencies in the troposphere, *J. Atmos. Chem., 18*, 171-210, 1994.

Schlager, H., P. Konopka, P. Schulte, U. Schumann, H. Ziereis, F. Arnold, M. Klemm, D. E. Hagen, P. D. Whitefield, and J. Ovarlez, In situ observations of airtraffic emission signatures in the North Atlantic flight corridor, *J. Geophys. Res., 102*, 10,739-10,750, 1997.

Schulte, P., and H. Schlager, In-flight measurements of cruise altitude nitric oxide emission indices of commercial jet aircraft, *Geophys. Res. Lett., 23*, 165-168, 1996.

Schumann, U., On the effect of emissions from aircraft engines on the state of the atmosphere, *Ann. Geophys., 12*, 365-384, 1994.

Schumann, U., On conditions for contrail formation from aircraft exhausts, *Meteorol. Z., 5*, 4-23, 1996.

Vilà-Guerau de Arellano, J., P. G. Duynkerke, and M. van Weele, Tethered-balloon measurements of actinic flux in a cloud-capped marine boundary layer, *J. Geophys. Res, 99*, 3699-3705, 1994.

Wuebbles, D. J., D. Maiden, R. K. Seals Jr., S. L. Baughcum, M. Metwally, and A. Mortlock, Emission scenarios developement: Report of the emission scenarios committee, *NASA Ref. Pub. 1313*, pp. 63-208, 1993.

S.L. Baughcum, Boeing Company, P.O. Box 3707, MS 6H-FC, Seattle, WA 98124. (e-mail: slb0347@o3.ca.boeing.com)

F. Deidewig, Deutsche Forschungsanstalt für Luft- und Raumfahrt, Institut für Antriebstechnik, Linder Höhe, D-51140 Köln, Germany. (e-mail: Frank.Deidewig@dlr.de)

P. Schulte, H. Schlager, H. Ziereis, and U. Schumann, Deutsche Forschungsanstalt für Luft- und Raumfahrt, Institut für Physik der Atmosphäre, Oberpfaffenhofen, D-82230 Wessling, Germany. (e-mail: Peter.Schulte@dlr.de; Hans.Schlager@dlr.de; Helmut.Ziereis@dlr.de; Ulrich.Schumann@dlr.de)

(Received October 11, 1996; revised April 21, 1997; accepted May 21, 1997.)